Supporting Information

Regulating the frontier orbital of iron phthalocyanine by nitrogen doped carbon nanosheets for improving oxygen reduction activity

Xilin Zhang[1,2], Rui Zheng[1], Qingfang Chang[1*], Zhongjun Ma[2*], Zongxian Yang[1*]
[1]School of Physics, Henan Key Laboratory of Photovoltaic Materials, Henan Normal University, 46 Jianshe Road, Xinxiang 453007, China
[2]Key Laboratory of Yellow River and Huai River Water Environmental and Pollution Control, Ministry of Education, School of Environment, Henan Normal University, Xinxiang 453007, China.
[*]Corresponding author: qingfangchang@163.com (Q Chang); mazhongjun81@sina.com (J Ma); yzx@htu.edu.cn (Z Yang).

1. Computational Methods

All the spin--polarized first-principles calculations were completed by the DMol^3 code embedded in Material studio.[1] The empirical dispersion-corrected density functional theory (DFT-D) was employed to handle the van-der-Waals (vdW) interactions.[2] The Perdeu–Burke–Ernzerhof (PBE) functional[3] within generalized gradient approximation (GGA)[4]was employed to describe the exchange correlation interactions. The interactions between valence electrons and ion-cores were treated by the DFT Semi-core Pseudopotential.[5] The double numerical plus polarization (DNP) basis was utilized to ensure the accuracy and decrease the computational cost.[6] During geometric and electronic optimizations, the convergence criterions were set to 10^{-6} Ha for energy and 0.002 Ha/Å for force. The smearing values were specified with 0.005 Ha to achieve fast convergence. Using the Monkhorst-Pack method,[7] the Brillouin zone was sampled with the 5 × 5 × 1 k-points grids for all calculations.

The computional hydrogen electrode model (CHE model) developed by Nørskov and coworkers[8, 9] was adopted to theoretically evaluate and compare the ORR activity of different systems. Taking standard hydrogen electrode(SHE) as the reference potential, the free energy of (H^++ e^-) is then equal to the free energy of 1/2 H_2; the stability of adsorbed oxygenate intermediates by water environment is modelled by the solvation effects and the implicit solvation model that describes the effect of electrostatic screening by water solvent is used here for simplification[10]; the effect of a bias on all states involving an electron in the electrode is calculated by –eU; and the pH effects were involved by correcting the free energy of H^+ ions according to the concentration dependence of the entropy:

$G(\mathrm{pH}) = -kT \ln[\mathrm{H^+}] = kT \ln 10 \times \mathrm{pH}$.

With these assumptions in mind, the adsorption free energies of oxygenates intermediates can be obtained by including the zero point energy (ZPE) and the entropy (S) corrections in equation

$$\triangle G_{ads} = \triangle E_{ads} + \triangle ZPE - T\triangle S \quad (4).$$

The $\triangle$ZPE could be obtained from the calculation of vibrational frequencies for the adsorbed species. The adsorption energy ($\triangle E_{ads}$) can be derived from following equations[9]:

$$\Delta E_{O*} = E_{O*} - E_{*} - \left[E_{H_2O} - E_{H_2}\right] \quad (1)$$

$$\Delta E_{OH*} = E_{OH*} - E_{*} - \left[E_{H_2O} - 1/2E_{H_2}\right] \quad (2)$$

$$\Delta E_{OOH*} = E_{OOH*} - E_{*} - \left[2E_{H_2O} - 3/2E_{H_2}\right] \quad (3)$$

in which the E_*, E_{OOH*}, E_{OH*}, and E_{O*} are the total energies of catalyst substrate without and with the adsorption of OOH, OH and O, respectively. E_{H_2O} and E_{H_2} are total energies of free H_2O and H_2 molecules in gas phases, respectively.

In alkaline media, the overall ORR could be expressed as:

$$O_2(g) + 2H_2O(l) + 4e^- \rightarrow 4OH^- \quad (5)$$

The elementary reaction steps along the concerted four-electron process are listed as below:

(i) $* + O_2(g) + H_2O(l) + e^- \rightarrow OOH^* + OH^-$

(ii) $OOH^* + e^- \rightarrow O^* + OH^-$

(iii) $O^* + H_2O(l) + e^- \rightarrow OH^* + OH^-$

(iv) $OH^* + e^- \rightarrow * + OH^-$

where * stands for the adsorption states. l and g refer to liquid and gas phases, respectively.

The change in Gibbs free energy (i.e., the reaction free energy barriers, $\triangle$G) for each reaction step is given by the equation[8]:

$$\triangle G = \triangle E + \triangle ZPE - T\triangle S + \triangle G_U + G(\mathrm{pH}) \quad (6)$$

where $\triangle E$ is reaction heats of a certain reaction step, $\triangle G_U = -eU$ with U being the electrode potential. The T is temperature. The free energy of O_2 was obtained from the reaction $O_2 + 2H_2 \rightarrow 2H_2O$ for which the free energy change is 4.92 eV. The overpotential could then be derived by[9]:

$$\eta = 1.23 - \min(\triangle G_i, \triangle G_{ii}, \triangle G_{iii}, \triangle G_{iv})/e \quad (7)$$

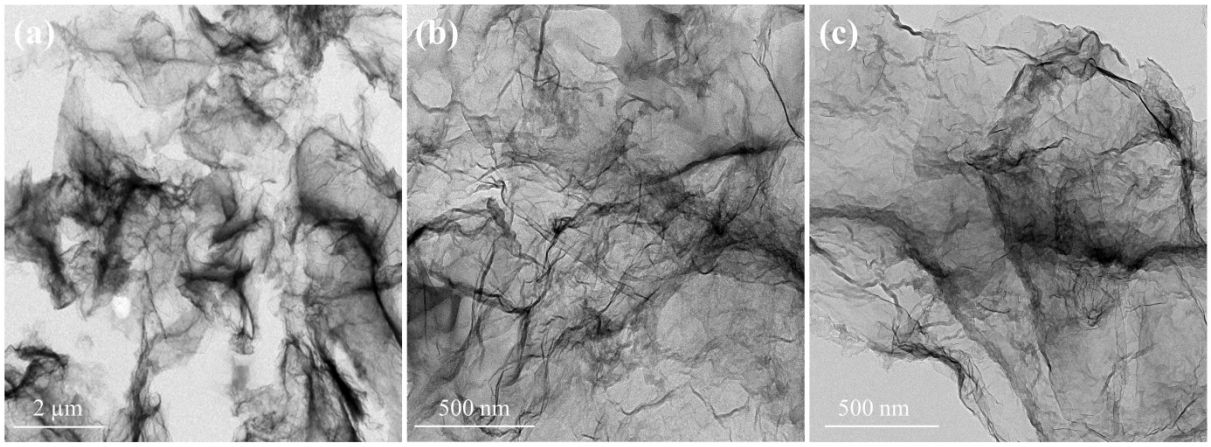

Figure S1. TEM images of N-CNSs at different magnifications.

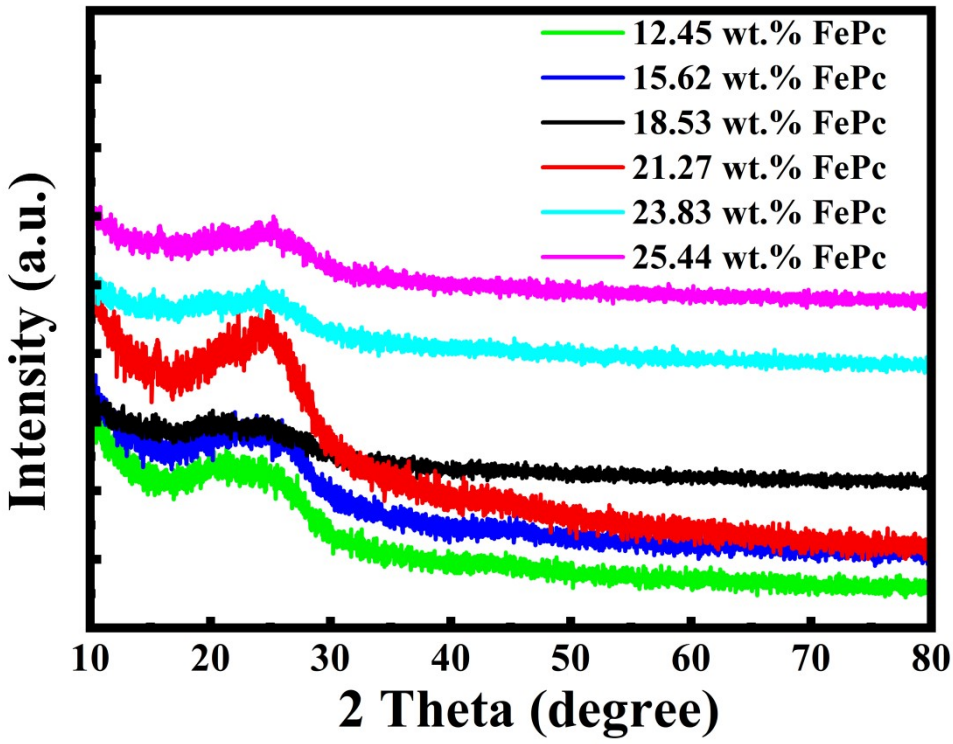

Figure S2. XRD of loaded iron phthalocyanine with different amounts.

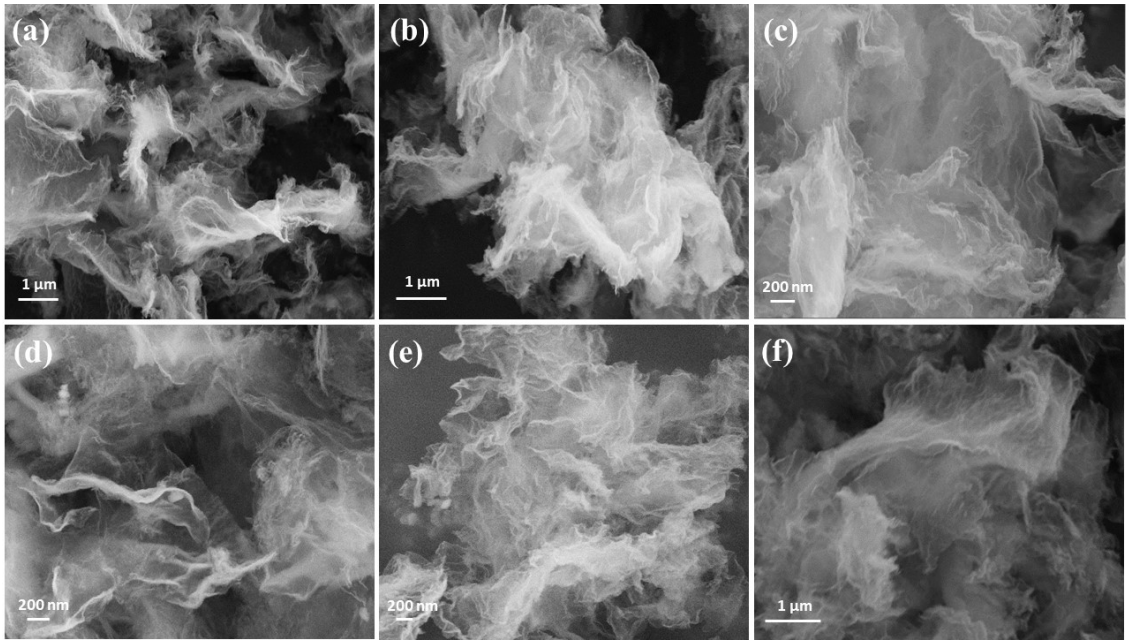

Figure S3. SEM of loaded iron phthalocyanine with different amounts.

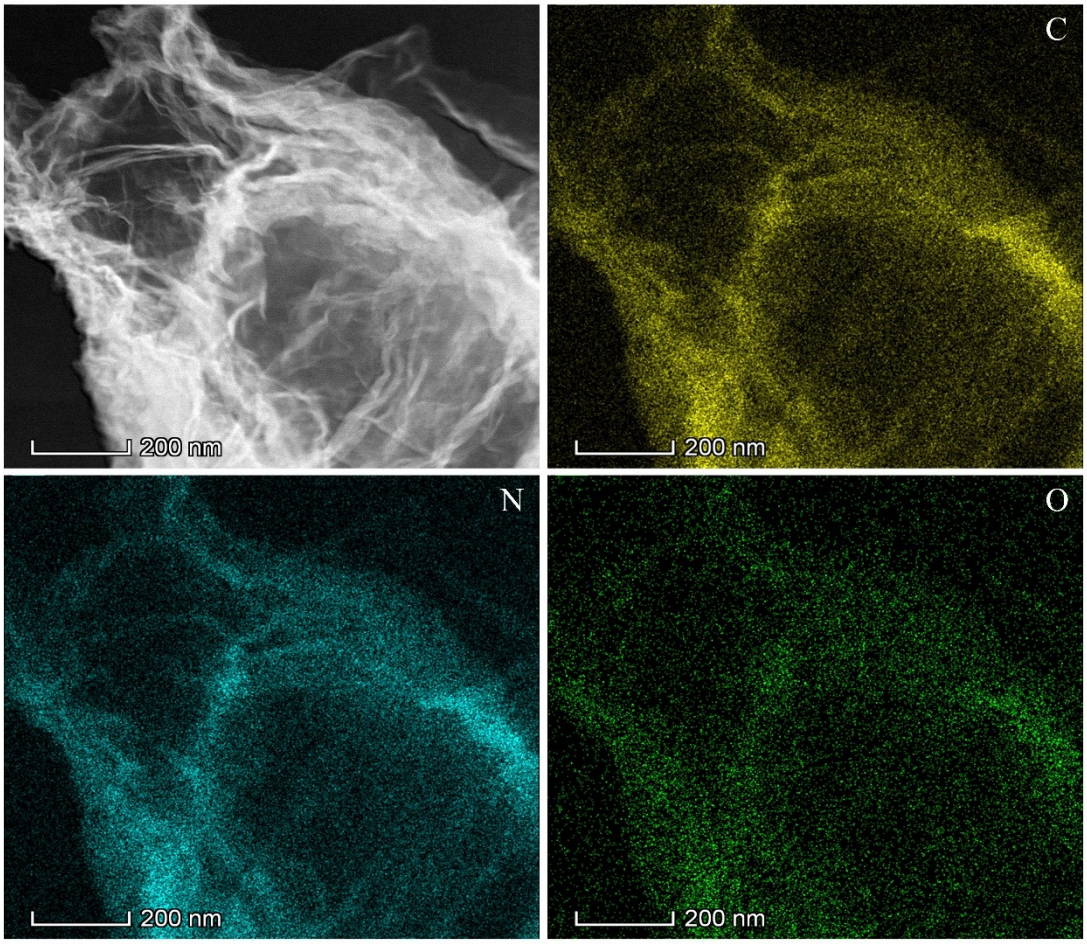

Figure S4. Elemental mappings of N-CNSs.

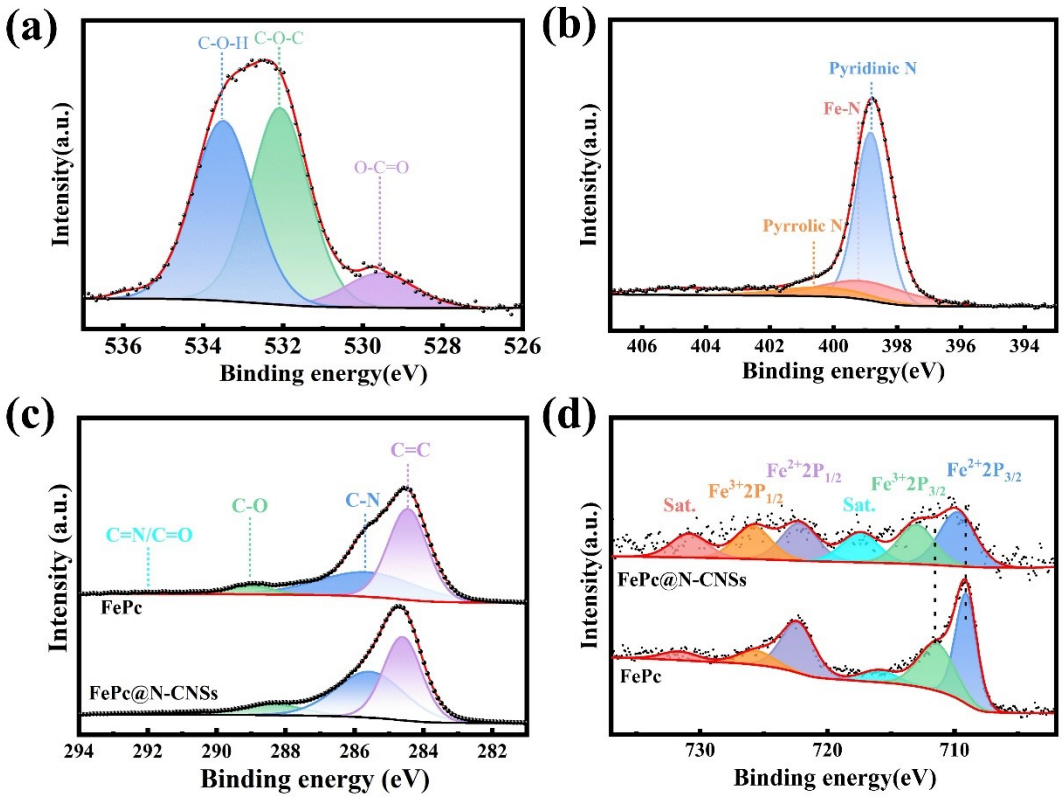

Figure S5. (a) High-resolution O 1s spectra of FePc. (b) N 1s spectra of FePc. (c) C 1s spectra of FePc and FePc@N-CNSs samples. (d) Fe 2p spectra of FePc and FePc@N-CNSs samples.

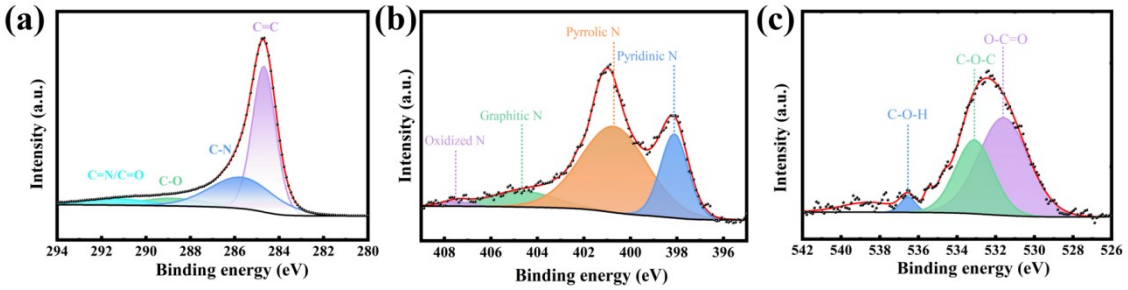

Figure S6. (a) High-resolution C 1s spectra. (b) N 1s and (c) O 1s spectra of N-CNSs samples.

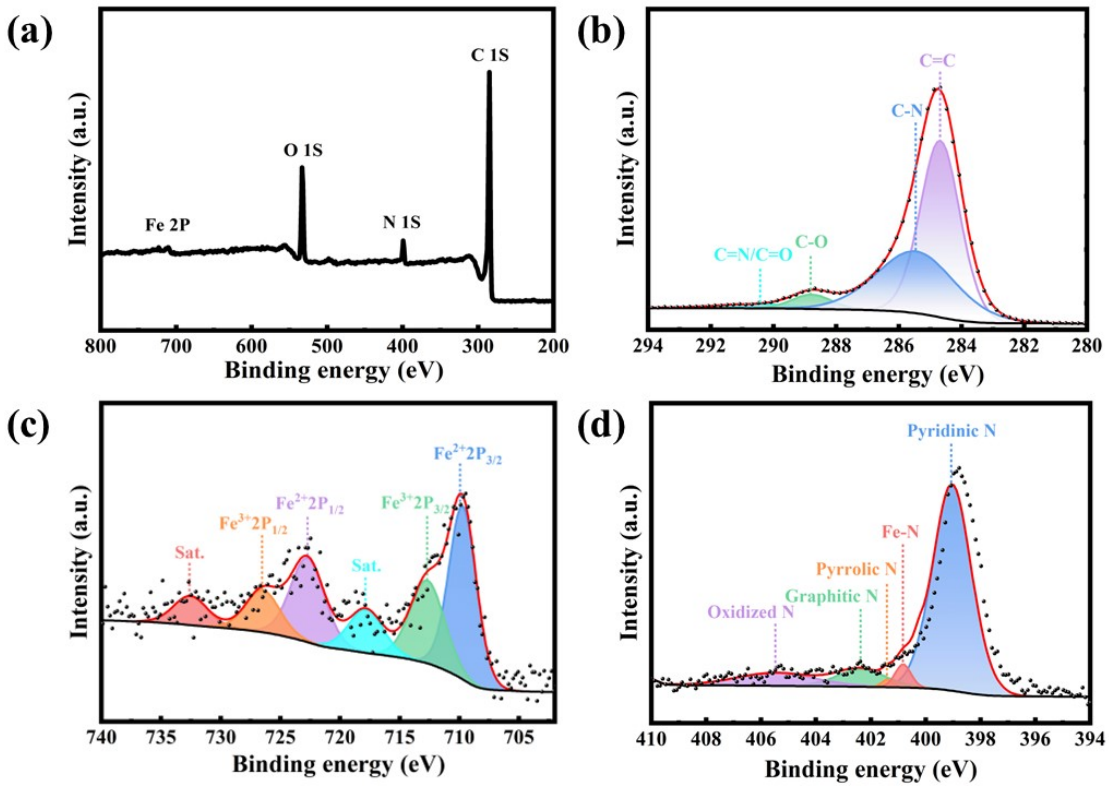

Figure S7. (a) XPS survey spectrum. (b) C 1s (c) Fe 2p and (d) N 1s spectra of FePc@XC72 samples.

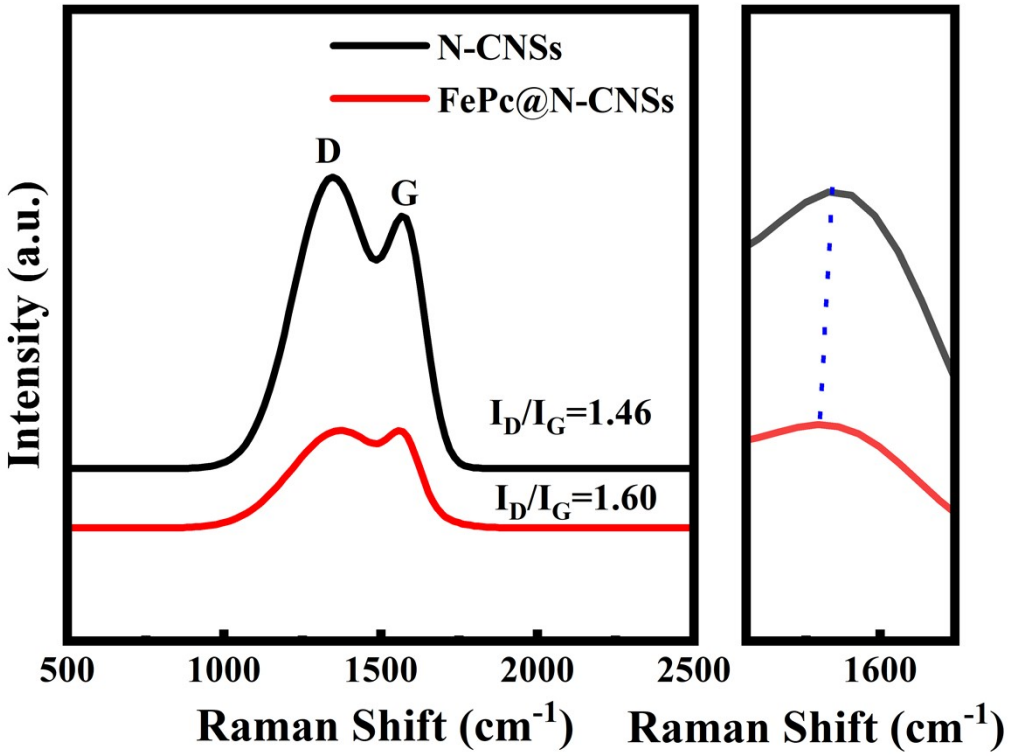

Figure S8. Raman spectra of the N-CNSs and FePc@N-CNSs.

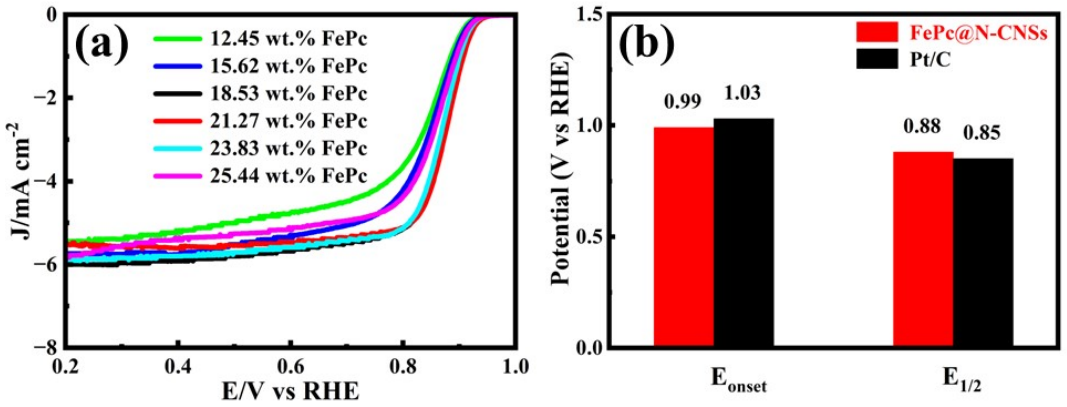

Figure S9. (a) ORR polarization curves of FePc@N-CNSs with different FePc loadings. (b) Onset potentials and half-wave potentials of FePc@N-CNSs and Pt/C.

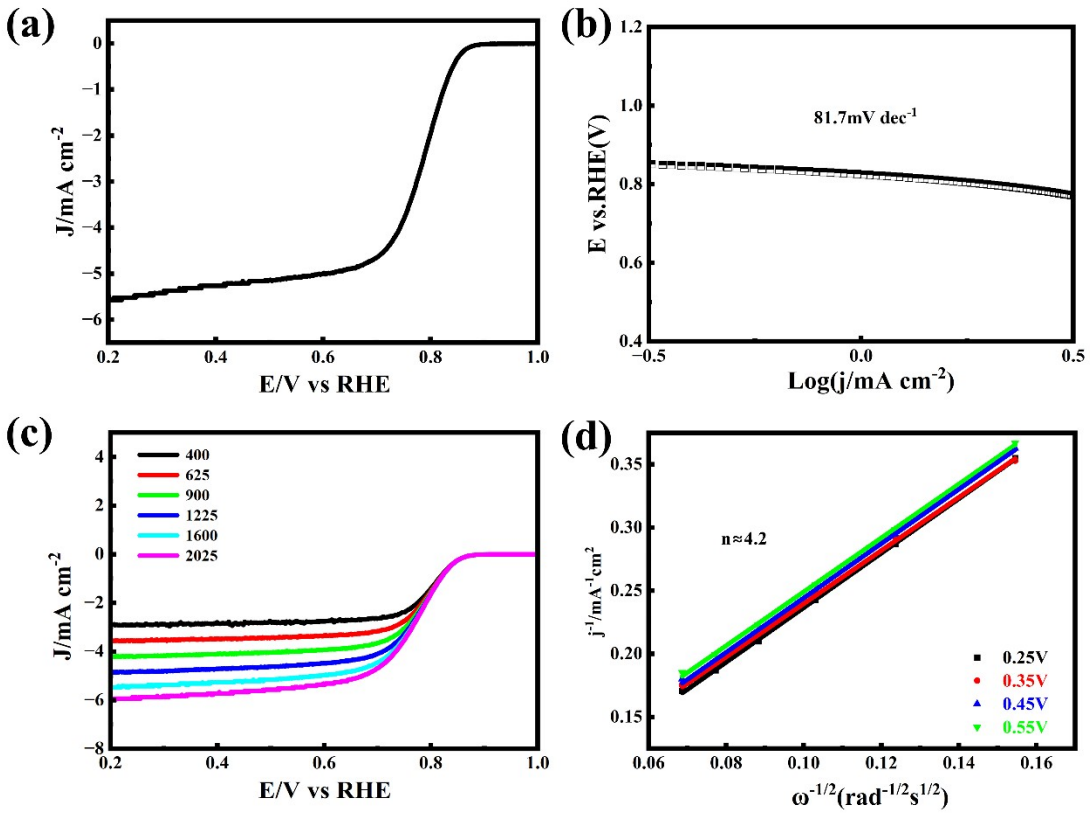

Figure S10. (a) ORR polarization curves of iron phthalocyanine loaded onto carbon black. (b) Tafel plots and (c) LSV curves of FePc@XC72 with a scan rate of 5 $mV \cdot s^{-1}$ at different rotation rates. (d) The K−L plots.

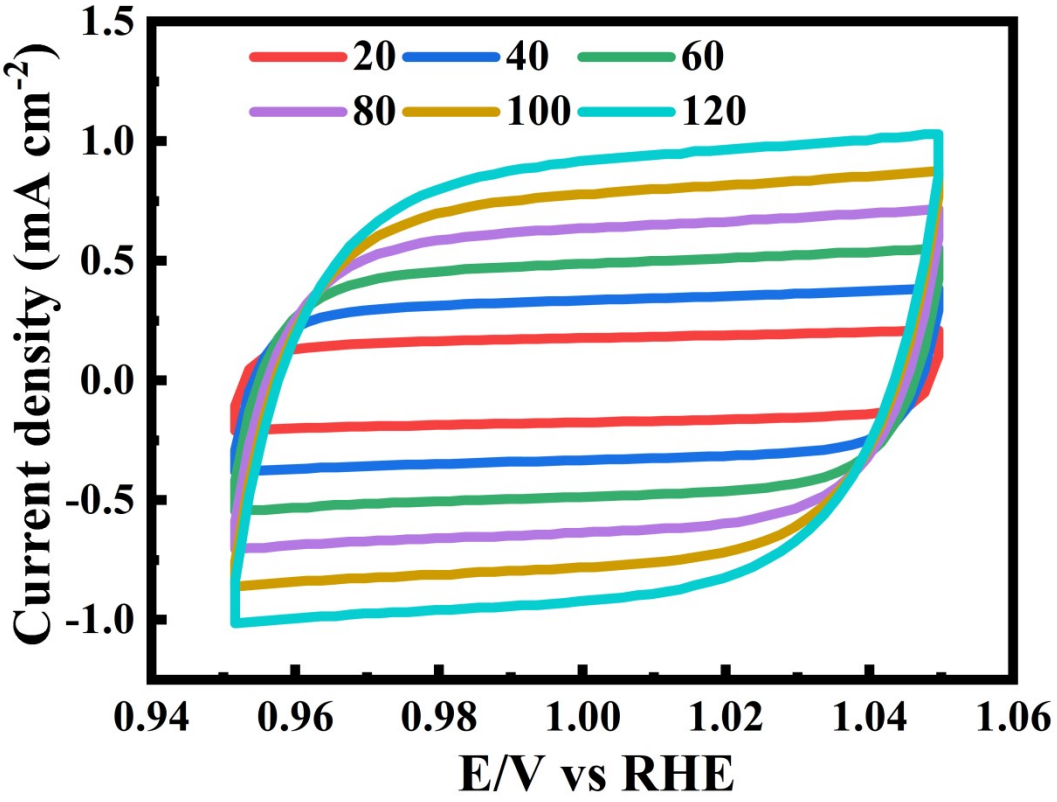

Figure S11. Cyclic voltammetry (CV) curves of FePc@N-CNSs at different scan rates ranging from 20 mV s^{-1} to 120 mV s^{-1} with a step of 20 mV s^{-1}.

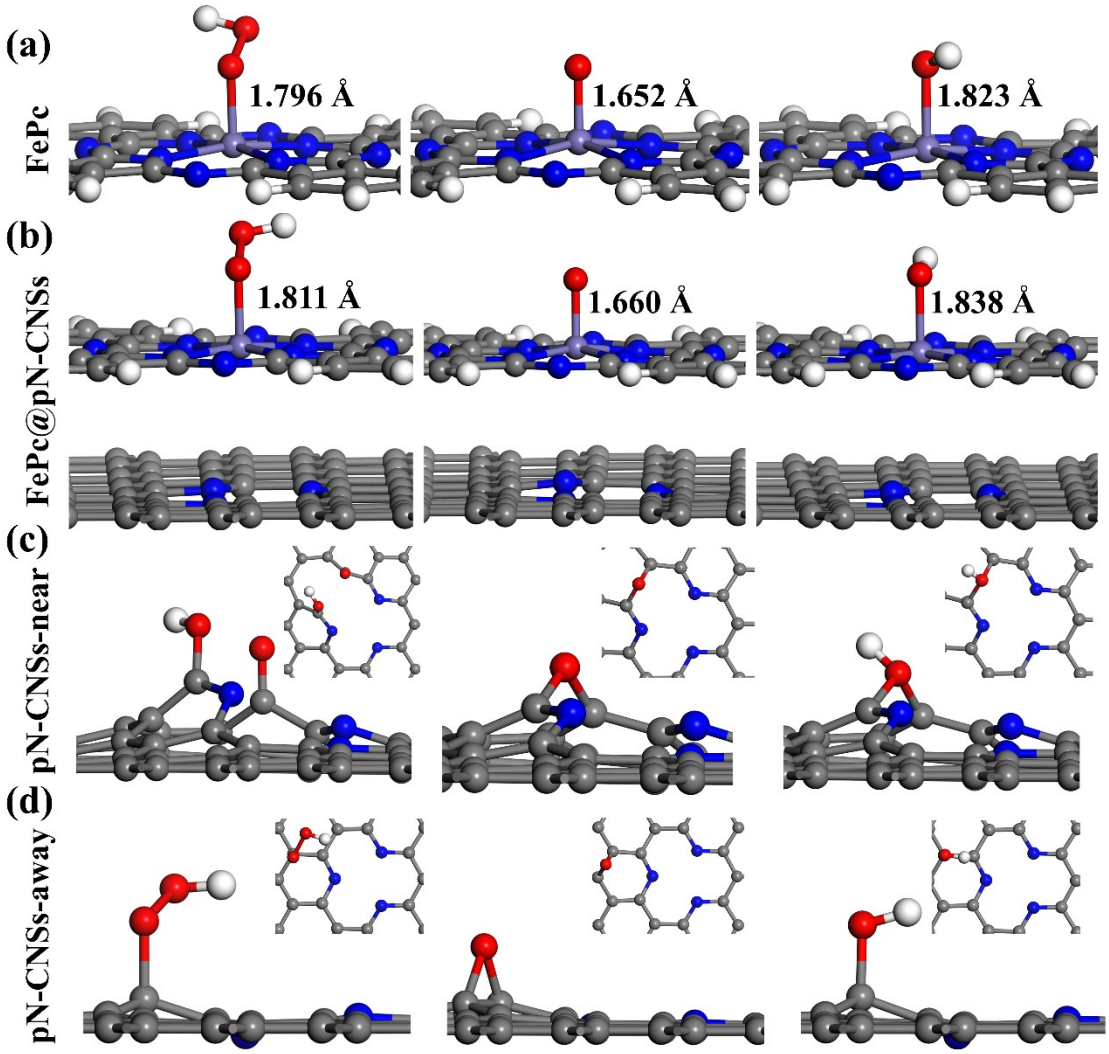

Figure S12. Adsorption configurations of intermediates on FePc (a), FePc@pN-CNSs (b) and pN-CNSs (c-d). Where pN-CNSs-near and pN-CNSs-away represent intermediates adsorb at C atom near and away from N atom, respectively.

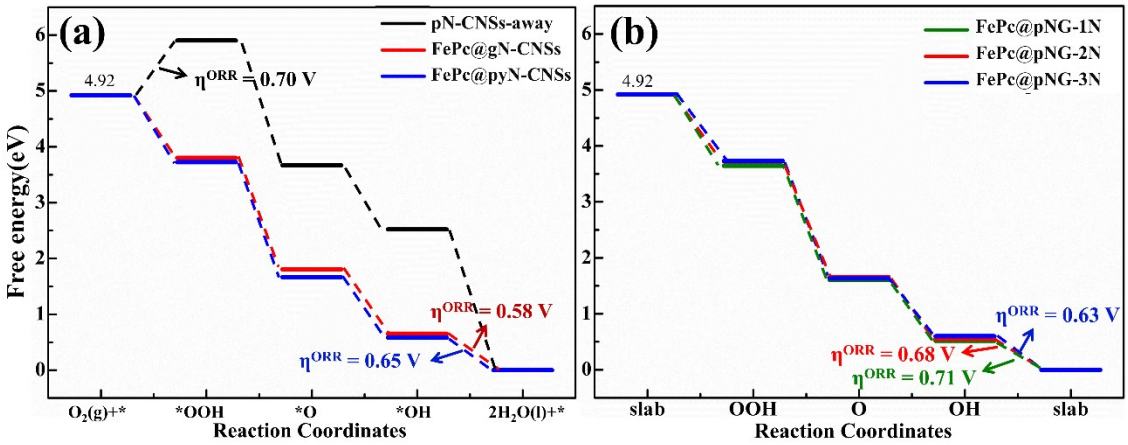

Figure S13. Gibbs free energy diagrams of ORR at U = 0 V for (a) pN-CNSs-away, FePc@gN-CNSs and FePc@pyN-CNSs systems, and (b) FePc@pNG-1N, FePc@pNG-2N, FePc@pNG-1N systems.

Table S1 Comparison of ORR activity of recently reported FePc-based samples

Samples	Onset potential (V)	Half-wave potential (V)	Limiting Diffusion Current Density (mA cm^{-2})	References
FePc@N-CNSs	0.99	0.88	5.8	This work
ER(FePc/GO)	0.97	0.86	5.31	[11]
FeAB–O	~0.98	0.90	~6.1	[12]
FePc&rGO	0.98	0.89	5.4	[13]
Fe-N-C-700	0.955	0.83	~5.5	[14]
Fe-SACs/NC	0.943	0.865	5.7	[15]
FePc/$Ti_3C_2T_x$	~0.96	0.886	~5.5	[16]
FePc-CNTs	0.937	0.858	5.33	[17]
FePc@N,P-DC	0.984	0.903	~5.7	[18]
FePc-R25	0.973	0.86	~5.8	[19]
FePc/CoPc HS	0.971	0.879	~5.7	[20]
FePc@HNSC	0.93	0.84	6.1	[21]
FePc-P/MWCNTs-A	0.979	0.902	5.42	[22]
FePc/GaS	0.97	0.87	~5.8	[23]
FePc@Co-SAs/PCNF	0.99	0.87	7.5	[24]
Pc-FePc/Mn-GCB	~0.98	0.88	~5.2	[25]
Fe/CNsh	1.00	0.87	6.2	[26]
FePc@NC-1000	0.99	0.86	5.96	[27]
D-MN_4-CNF-IL-A	0.98	0.857	~6.5	[28]
FeCo–C/N s	~0.95	0.864	~4.9	[29]

FeNiN-MWCNT	0.93	0.86	~6.2	[30]
FeNi-COP-800	0.95	0.80	~5.6	[31]
TiCDC/CNT (1:3)/FePc	0.93	0.77	~5.8	[32]
FePc/PSAC-3/1	0.94	0.85	5.42	[33]
FeCu SACs/NC	0.84	0.75	7.27	[34]
CAN-Pc (Fe/Co)	1.04	0.84	5.23	[35]

Reference

[1]·Delley, B., From molecules to solids with the $DMol_3$ approach. *The Journal of Chemical Physics* **2000,** *113* (18), 7756-7764.

[2]·Grimme, S., Accurate description of van der Waals complexes by density functional theory including empirical corrections. *Journal of Computational Chemistry* **2004,** *25* (12), 1463-1473.

[3]·Ernzerhof, M.; Scuseria, G. E., Assessment of the Perdew–Burke–Ernzerhof exchange-correlation functional. *The Journal of Chemical Physics* **1999,** *110* (11), 5029-5036.

[4]·Perdew, J. P.; Burke, K.; Ernzerhof, M., Generalized Gradient Approximation Made Simple. *Physical Review Letters* **1996,** *77* (18), 3865-3868.

[5]·Delley, B., Hardness conserving semilocal pseudopotentials. *Physical Review B* **2002,** *66* (15), 155125.

[6]·Koelling, D. D.; Harmon, B. N., A technique for relativistic spin-polarised calculations. *Journal of Physics C: Solid State Physics* **1977,** *10* (16), 3107.

[7]·Monkhorst, H. J.; Pack, J. D., Special points for Brillouin-zone integrations. *Physical Review B* **1976,** *13* (12), 5188-5192.

[8]·Nørskov, J. K.; Rossmeisl, J.; Logadottir, A.; Lindqvist, L.; Kitchin, J. R.; Bligaard, T.; Jónsson, H., Origin of the Overpotential for Oxygen Reduction at a Fuel-Cell Cathode. *The Journal of Physical Chemistry B* **2004,** *108* (46), 17886-17892.

[9]·Man, I.; Su, H.-Y.; Calle-Vallejo, F.; Hansen, H.; Hansen, A.; Nilay; Inoglu, G.; Kitchin, J.; Jaramillo, T.; Nørskov, J.; Rossmeisl, J., Universality in Oxygen Evolution Electrocatalysis on Oxide Surfaces. *ChemCatChem* **2011,** *3*, 1159.

[10]·Di Liberto, G.; Pacchioni, G.; Shao-Horn, Y.; Giordano, L., Role of Water Solvation on the Key Intermediates Catalyzing Oxygen Evolution on RuO_2. *The Journal of Physical Chemistry C* **2023,** *127* (21), 10127-10133.

[11]·Irisa, K.; Hatakeyama, K.; Yoshimoto, S.; Koinuma, M.; Ida, S., Oxygen reduction reaction activity of an iron phthalocyanine/graphene oxide nanocomposite. *RSC Advances* **2021,** *11* (26), 15927-15932.

[12]·Chen, K.; Liu, K.; An, P.; Li, H.; Lin, Y.; Hu, J.; Jia, C.; Fu, J.; Li, H.; Liu, H.; Lin, Z.; Li, W.; Li, J.; Lu, Y.-R.; Chan, T.-S.; Zhang, N.; Liu, M., Iron phthalocyanine with coordination induced electronic localization to boost oxygen reduction reaction. *Nature Communications* **2020,** *11* (1), 4173.

[13]·Mei, Z.-y.; Cai, S.; Zhao, G.; Jing, Q.; Sheng, X.; Jiang, J.; Guo, H., Understanding electronic configurarions and coordination environment for enhanced ORR process and improved Zn-

air battery performance. *Energy Storage Materials* **2022,** *50*, 12-20.
[14] Chen, T.; Wu, J.; Zhu, C.; Liu, Z.; Zhou, W.; Zhu, C.; Guan, C.; Fang, G., Rational design of iron single atom anchored on nitrogen doped carbon as a high-performance electrocatalyst for all-solid-state flexible zinc-air batteries. *Chemical Engineering Journal* **2021,** *405*, 125956.
[15] Liu, M.; Li, N.; Cao, S.; Wang, X.; Lu, X.; Kong, L.; Xu, Y.; Bu, X.-H., A "Pre-Constrained Metal Twins" Strategy to Prepare Efficient Dual-Metal-Atom Catalysts for Cooperative Oxygen Electrocatalysis. *Advanced Materials* **2022,** *34* (7), 2107421.
[16] Li, Z.; Zhuang, Z.; Lv, F.; Zhu, H.; Zhou, L.; Luo, M.; Zhu, J.; Lang, Z.; Feng, S.; Chen, W.; Mai, L.; Guo, S., The Marriage of the FeN_4 Moiety and MXene Boosts Oxygen Reduction Catalysis: Fe 3d Electron Delocalization Matters. *Advanced Materials* **2018,** *30* (43), 1803220.
[17] Yan, X.; Xu, X.; Zhong, Z.; Liu, J.; Tian, X.; Kang, L.; Yao, J., The effect of oxygen content of carbon nanotubes on the catalytic activity of carbon-based iron phthalocyanine for oxygen reduction reaction. *Electrochimica Acta* **2018,** *281*, 562-570.
[18] Cheng, W.; Yuan, P.; Lv, Z.; Guo, Y.; Qiao, Y.; Xue, X.; Liu, X.; Bai, W.; Wang, K.; Xu, Q.; Zhang, J., Boosting defective carbon by anchoring well-defined atomically dispersed metal-N_4 sites for ORR, OER, and Zn-air batteries. *Applied Catalysis B: Environmental* **2020,** *260*, 118198.
[19] Guo, J.; Yan, X.; Liu, Q.; Li, Q.; Xu, X.; Kang, L.; Cao, Z.; Chai, G.; Chen, J.; Wang, Y.; Yao, J., The synthesis and synergistic catalysis of iron phthalocyanine and its graphene-based axial complex for enhanced oxygen reduction. *Nano Energy* **2018,** *46*, 347-355.
[20] Ma, Y.; Li, J.; Liao, X.; Luo, W.; Huang, W.; Meng, J.; Chen, Q.; Xi, S.; Yu, R.; Zhao, Y.; Zhou, L.; Mai, L., Heterostructure Design in Bimetallic Phthalocyanine Boosts Oxygen Reduction Reaction Activity and Durability. *Advanced Functional Materials* **2020,** *30* (50), 2005000.
[21] Luo, Y.; Chen, Y.; Xue, Y.; Chen, J.; Wang, G.; Wang, R.; Yu, M.; Zhang, J., Electronic Structure Regulation of Iron Phthalocyanine Induced by Anchoring on Heteroatom-Doping Carbon Sphere for Efficient Oxygen Reduction Reaction and Al–Air Battery. *Small* **2022,** *18* (2), 2105594.
[22] Mei, Z.-y.; Cai, S.; Zhao, G.; Zou, X.; Fu, Y.; Jiang, J.; An, Q.; Li, M.; Liu, T.; Guo, H., Boosting the ORR active and Zn-air battery performance through ameliorating the coordination environment of iron phthalocyanine. *Chemical Engineering Journal* **2022,** *430*, 132691.
[23] Zhuang, Z.; Xia, L.; Huang, J.; Zhu, P.; Li, Y.; Ye, C.; Xia, M.; Yu, R.; Lang, Z.; Zhu, J.; Zheng, L.; Wang, Y.; Zhai, T.; Zhao, Y.; Wei, S.; Li, J.; Wang, D.; Li, Y., Continuous Modulation of Electrocatalytic Oxygen Reduction Activities of Single-Atom Catalysts through p-n Junction Rectification. *Angewandte Chemie International Edition* **2023,** *62* (5), e202212335.
[24] Wang, Y.; Li, K.; Cheng, R.; Xue, Q.; Wang, F.; Yang, Z.; Meng, P.; Jiang, M.; Zhang, J.; Fu, C., Enhanced electronic interaction between iron phthalocyanine and cobalt single atoms promoting oxygen reduction in alkaline and neutral aluminum-air batteries. *Chemical Engineering Journal* **2022,** *450*, 138213.
[25] Zhang, Z.; Dou, M.; Ji, J.; Wang, F., Phthalocyanine tethered iron phthalocyanine on graphitized carbon black as superior electrocatalyst for oxygen reduction reaction. *Nano Energy* **2017,** *34*, 338-343.
[26] Fang, C.; Yi, Q.; Chen, A.; Wang, Y.; Wang, Y.; Li, X., Fabrication of FeCo/Multidimensional Carbon-Based Nanocomposites as Excellent Cathodic Catalysts of Zn-Air

Battery. *Journal of The Electrochemical Society* **2022,** *169* (11), 110538.
[27] Dong, A.; Lin, Y.; Guo, Y.; Chen, D.; Wang, X.; Ge, Y.; Li, Q.; Qian, J., Immobilization of iron phthalocyanine on MOF-derived N-doped carbon for promoting oxygen reduction in zinc-air battery. *Journal of Colloid and Interface Science* **2023,** *650*, 2056-2064.
[28] Muuli, K.; Sokka, A.; Mooste, M.; Lilloja, J.; Gudkova, V.; Käärik, M.; Otsus, M.; Kikas, A.; Kisand, V.; Tamm, A.; Leis, J.; Krumme, A.; Holdcroft, S.; Zagal, J. H.; Tammeveski, K., Iron and cobalt phthalocyanine embedded electrospun carbon nanofiber-based catalysts for anion exchange membrane fuel cell cathode. *Journal of Catalysis* **2023,** *422*, 117-130.
[29] Zhang, C.; Yang, H.; Zhong, D.; Xu, Y.; Wang, Y.; Yuan, Q.; Liang, Z.; Wang, B.; Zhang, W.; Zheng, H.; Cheng, T.; Cao, R., A yolk–shell structured metal–organic framework with encapsulated iron-porphyrin and its derived bimetallic nitrogen-doped porous carbon for an efficient oxygen reduction reaction. *Journal of Materials Chemistry A* **2020,** *8* (19), 9536-9544.
[30] Kumar, Y.; Kibena-Põldsepp, E.; Kozlova, J.; Rähn, M.; Treshchalov, A.; Kikas, A.; Kisand, V.; Aruväli, J.; Tamm, A.; Douglin, J. C.; Folkman, S. J.; Gelmetti, I.; Garcés-Pineda, F. A.; Galán-Mascarós, J. R.; Dekel, D. R.; Tammeveski, K., Bifunctional Oxygen Electrocatalysis on Mixed Metal Phthalocyanine-Modified Carbon Nanotubes Prepared via Pyrolysis. *ACS Applied Materials & Interfaces* **2021,** *13* (35), 41507-41516.
[31] Liao, Z.; Wang, Y.; Wang, Q.; Cheng, Y.; Xiang, Z., Bimetal-phthalocyanine based covalent organic polymers for highly efficient oxygen electrode. *Applied Catalysis B: Environmental* **2019,** *243*, 204-211.
[32] Praats, R.; Käärik, M.; Kikas, A.; Kisand, V.; Aruväli, J.; Paiste, P.; Merisalu, M.; Leis, J.; Sammelselg, V.; Zagal, J. H.; Holdcroft, S.; Nakashima, N.; Tammeveski, K., Electrocatalytic oxygen reduction reaction on iron phthalocyanine-modified carbide-derived carbon/carbon nanotube composite electrocatalysts. *Electrochimica Acta* **2020,** *334*, 135575.
[33] Feng, Y.; Tian, G.; Peng, Q.; Wu, Y.; Li, Y.; Luo, X.; Han, Y.; Li, Q., Fe-N Doped Peanut Shell Activated Carbon as a Superior Electrocatalyst for Oxygen Reduction and Cathode Catalyst for Zinc-Air Battery. *ChemElectroChem* **2021,** *8* (24), 4797-4803.
[34] Liu, H.; Jiang, L.; Wang, Y.; Wang, X.; Khan, J.; Zhu, Y.; Xiao, J.; Li, L.; Han, L., Boosting oxygen reduction with coexistence of single-atomic Fe and Cu sites decorated nitrogen-doped porous carbon. *Chemical Engineering Journal* **2023,** *452*, 138938.
[35] Yang, S.; Yu, Y.; Dou, M.; Zhang, Z.; Dai, L.; Wang, F., Two-Dimensional Conjugated Aromatic Networks as High-Site-Density and Single-Atom Electrocatalysts for the Oxygen Reduction Reaction. *Angewandte Chemie International Edition* **2019,** *58* (41), 14724-14730.